# Sunlight Noise Mitigation in FMCW LiDAR Using FADOF

Longfei Yin, Wei Tang, Ziwei Geng, Haodi Zhan, Lei Chen, Dasheng Qian, Guohua Wu, and Bin Luo

***Abstract*—This paper examines the potential of utilizing a Faraday anomalous dispersion optical filter (FADOF) to enhance noise reduction in a FMCW LiDAR (Frequency-Modulated Continuous-Wave Laser Detection And Ranging) system. While the FMCW LiDAR itself demonstrates a certain level of robustness, it may fail to operate effectively in the presence of significant background noise interference. To address this challenge, we have proposed a validation experiment utilizing FADOF technology. Specifically, we have introduced a FADOF component at the optical receiving end of the FMCW LiDAR, and we have implemented a dynamic frequency stabilization method that combines frequency stability with frequency modulation for the laser source in the transmitter. By integrating FADOF into the FMCW LiDAR system to mitigate external noise, we conduct indoor and outdoor validation experiments. In the outdoor experiment, we introduce real sunlight background noise into the system, allowing it to directly illuminate the receiver. We then filter the light using FADOF and a 10 nm filter, separately. The experimental results confirm that the FMCW LiDAR system, when equipped with FADOF, can operate normally in intense background light noise, with a noise resistance capability at least twice as effective as the 10 nm filter. Additionally, the system achieves a detection range of at least 17 meters under direct sunlight conditions. This study has the potential to extend the application of LiDAR systems to more extreme environments with strong background noise, enabling their functionality in a broader range of scenarios.**

***Index Terms*—Faraday anomalous dispersion optical filter (FADOF), frequency-modulated continuous-wave (FMCW), laser frequency stabilization, noise suppression.**

## I. Introduction

LIDAR (Laser Detection And Ranging) serves as an active remote sensing technology that employs lasers to detect targets and gather distance, speed, and orientation information from the resulting reflected light. This approach boasts notable advantages such as high resolution, compact size, and remarkable resistance to interference [1]. LiDAR has found applications in diverse fields including surveying and mapping [2], forestry [3], topography [4], atmospheric detection [5], and three-dimensional imaging [6].

Amidst the progression of various technologies, FMCW (Frequency-Modulated Continuous-Wave) LiDAR has gained increasing attention. When contrasted with pulse LiDAR, a direct detection approach, FMCW LiDAR holds several advantages such as an extensive ranging range, high range resolution, and robust noise resistance [7], [8], [9], [10], [11].

While FMCW method inherently possesses robustness, the quest to further fortify its noise immunity remains a pivotal research concern. In 2016, S. Ayhan. tested the effects of FM nonlinearity, phase noise, and SNR on FMCW radar, and presented simulation and experimental results [12]. H. Tian from the University of Defense Science and Technology took on the challenge of reducing strong noise in compact FMCW SAR systems. They came up with a solution using the fast Fourier transform (FFT) technique [13]. Moving to 2019, K. Siddiq from the University of Bath introduced a phase noise theory tailored for FMCW radar systems. This theory showcased the impact of phase noise and presented novel methods for mitigating phase noise effects [14]. Jumping ahead to 2020, R. Wang of Xidian University presented an FMCW radar signal ensemble empirical mode decomposition (EEMD) denoising approach. This method, based on singular spectral constraints, effectively filtered out a limited number of useful signals while suppressing a larger amount of noise [15].

LiDAR utilizes light waves to detect objects and analyze their motion with greater accuracy than microwave band radar. Unlike the latter, LiDAR has fewer sources of noise. However, under extreme conditions such as direct sunlight, optical noise can also impair the function of a FMCW LiDAR. Our research endeavors focus on devising and empirically analyzing a fresh strategy to counteract external noise in FMCW LiDAR. This novel approach uses the power of the Faraday anomalous dispersion filter (FADOF), known for its exceptional attributes of high transmittance, narrow bandwidth, and impressive noise rejection ratio [16], [17], Currently, FADOF has been developed and applied on alkali metal atoms such as Na (589 nm) [18], K (767 nm, 770 nm) [19], and its working range covers numerous frequency bands between 400 nm and 1600 nm [16], [20]. These qualities have already propelled FADOF to prominence within the optical domain, demonstrating exceptional performance. Despite its notable applications in diverse fields like thermometric LiDAR [21], [22], laser communication [23], Faraday laser [24], and ghost imaging [25], Till now,

Manuscript received 9 December 2023; revised 2 April 2024; accepted 10 April 2024. Date of publication 12 April 2024; date of current version 22 April 2024. This work was supported in part by the National Natural Science Foundation of China under Grant 62071059 and Grant 61801042, and in part by BUPT Excellent Ph.D. Students Foundation under Grant CX2023137. *(Corresponding author: Longfei Yin.)*

Longfei Yin, Wei Tang, Ziwei Geng, Haodi Zhan, Lei Chen, Dasheng Qian, Guohua Wu, and Bin Luo are with the School of Electronic Engineering, Beijing University of Posts and Telecommunications, Beijing 100876, China, and also with the State Key Laboratory of Information Photonics and Optical Communications, Beijing University of Posts and Telecommunications, Beijing 100876, China (e-mail: yinlongfei@bupt.edu.cn).

Digital Object Identifier 10.1109/JPHOT.2024.3388326

FADOF has yet to make an appearance within the realm of FMCW LiDAR.

In the research of modern FMCW LiDAR, the widely used wavelength is 1550 nm. This wavelength not only meets the eye safety requirements but also exhibits much weaker sunlight noise compared to the visible light spectrum. The fabrication processes for laser sources, modulators, detectors, and other optical components in the 1550 nm wavelength band are highly mature, with a wide range of available products, making them very suitable for the development of modern FMCW LiDAR systems. A certain type of Rb-ESFADOF (Excited states FADOF) enables ultra-narrowband transmission at 1529 nm [20], which is in proximity to the 1550 nm band. However, due to the lack of laser sources at this wavelength in our laboratory, direct construction of a LiDAR experiment in this band is not feasible. Consequently, we leverage existing equipment to design a validation experiment at 766.7 nm, integrating FADOF into an FMCW LiDAR system. The objective is to validate the functionality of an FMCW LiDAR enhanced with FADOF in environments affected by direct sunlight interference.

In this experiment, it's essential to ensure both laser linear frequency modulation and that the frequency remains within the passband of FADOF. Considering FADOF's narrow bandwidth characteristics, we employ a dynamic frequency stabilization method that combines frequency range locking and modulation to meet these two requirements. We first conduct an experiment using fluctuating background light noise indoors, and then test it under real sunlight conditions outdoors. The results from both validation experiments show that even in situations with intense and fluctuating background light, and in extreme cases where sunlight directly interferes with the LiDAR system, an FMCW LiDAR system equipped with FADOF can accurately measure the distance to targets. For instance, during early mornings or evenings when the sun is low, automotive LiDAR systems may struggle with strong sunlight interference, causing reduced visibility or blind spots. Similarly, LiDAR systems used for upward-facing applications may also have blind spots due to sunlight. This study suggests that FADOF-based FMCW LiDAR holds promise for effectively operating in such extreme scenarios.

## II. Indoor Experiment

### A. Indoor Experimental Setup

Optical experiments related to FADOF often employ tunable single-frequency diode lasers within specific wavelength ranges. Internal modulation finds straightforward implementation in such setups, thus we select the internal modulation approach for this experimentation. We have a K-FADOF, with a transmission wavelength of 766.7 nm, which matches the K atom's D2 line. Additionally, we have a laser with the same matching wavelength, which has the characteristics of high power and large electrical tuning range up to 50 GHz. So we build a FMCW LiDAR system at 766.7 nm.

As depicted in Fig. 1, the complete system comprises a frequency stabilization section and an FMCW LiDAR section. After the 766.7 nm laser is emitted, it is divided into two channels by BS1. One with strong laser power is used for FMCW LiDAR ranging experiment and the other one with weak laser power is used for frequency stabilization.

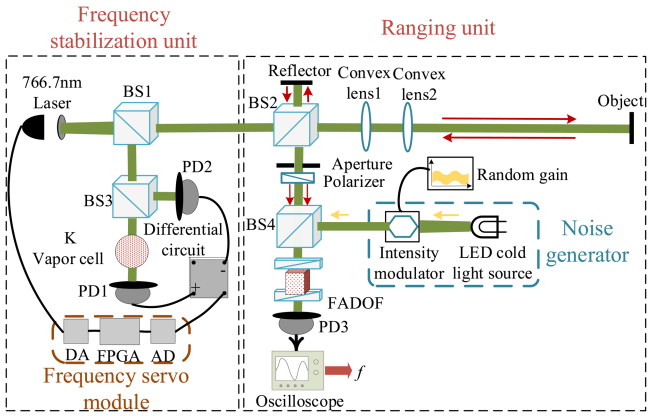


Fig. 1. Indoor experimental setup. BS1, BS2, BS3 and BS4 represent beam splitters. PD1, PD2 and PD3 represent photodetectors. A field programmable gate array (FPGA), an analog to digital (AD) converter and a digital to analog (DA) converter are used to control the laser frequency, thus forming a frequency servo module.

With in the frequency stabilization unit, the vapor cell contains K atoms, and is utilized for the frequency reference. The laser with atomic vapor absorbed and that without are detected by PD1 and PD2, and travel through the differential circuit and enters the frequency servo module, which modulates the laser's frequency.

The laser signal with linear frequency modulation is split into two beams by BS2. Within the ranging unit, one beam is directed through lens1 and lens2 to be collimated, aimed at the object, and then returns. The other beam is directly reflected by a local reflector and subsequently recombined into a single beam by BS2. The combined light beam passes through a polarizer, and one single linear polarization component is selected for beat frequency. Then, the beat frequency signal is mixed with the external noise generated by the noise generator module, prior to reaching the FADOF. Lastly, the beat frequency signal combined with noise, passes FADOF and is received by PD3. After the optical signal is converted into an electrical signal, it is connected to an oscilloscope, produced by KEYSIGHT, for observation and spectral analysis.

### B. FADOF and the Laser Modulating

Illustrated in Fig. 2(a), the FADOF configuration incorporates a pair of orthogonal polarizers alongside a K vapor cell positioned within a longitudinal magnetic field. P1 serves for polarization, while P2 is designated for polarization detection. The polarizer's extinction ratio stands at approximately $10^{-5}$. Subsequent to traversing the central atomic vapor cell, light exhibiting wavelengths distant from the atomic resonance line encounters another orthogonal polarizer at the rear, leading to blockage. Conversely, incident light closely aligned with the atom's resonant frequency undergoes polarization rotation and is thus transmitted. Fig. 2(b) shows the energy levels of K D2 line. The K atom's D2 line corresponds to the transition between the $4^2S_{1/2}$ and $4^2P_{3/2}$

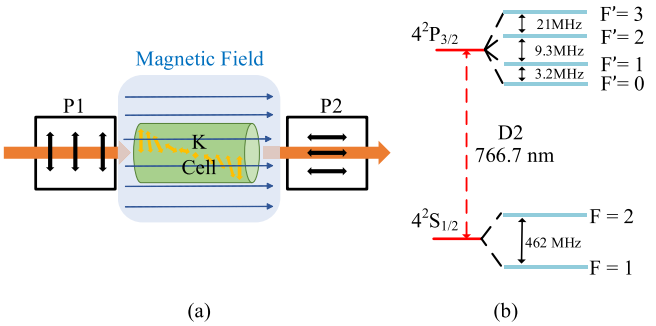


Fig. 2. Introduction to FADOF: (a) Working principle diagram of FADOF. P1 and P2 represent two orthogonal polarizers. The yellow arrow represents the polarization direction of light; (b) Energy level structure diagram of K atom [19].

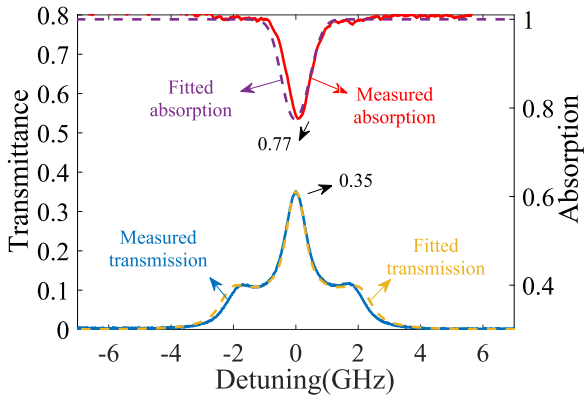


Fig. 3. Absorption lines of K atom without magnetic field at 43.0° and transmissions of K-FADOF. Experimental and theoretical filter transmissions for D2 line at an axial magnetic field of 682 Gs with a 3.5 cm cell at 80.0°C. The full width at half maximum is 1.05 GHz.

states, with a resonant wavelength of approximately 766. 7 nm.

Fig. 3 presents the transmission spectrum of K-FAODF near the D2 line and the absorption spectrum of K atom's D2 line. The frequency center point depicted in the graph, also known as the 0-detuning position, corresponds to the frequency of 766.7 nm wavelength light. The solid lines in the figure represent the actual measured spectra, while the dashed lines show the fit spectra obtained by multiplying the theoretical spectra calculated using ElecSus [26], [27] by the attenuation of the optical components. It's evident that the absorption spectrum and transmission spectrum exhibit highly congruent shapes with their respective theoretical counterparts. The central peak full width at half maximum (FWHM) of the FADOF transmission spectrum is approximately 1.05 GHz (2.1 pm). Due to this narrowband characteristic, if laser frequency is not locked, it's susceptible to drift out of the transmission band. Therefore, the signal laser cannot operate in free mode. Given that the frequency of the FADOF transmission peak aligns with the frequency of the K atom's D2 line absorption peak, locking the laser frequency to the D2 line absorption peak ensures that the laser frequency remains within the FADOF passband.

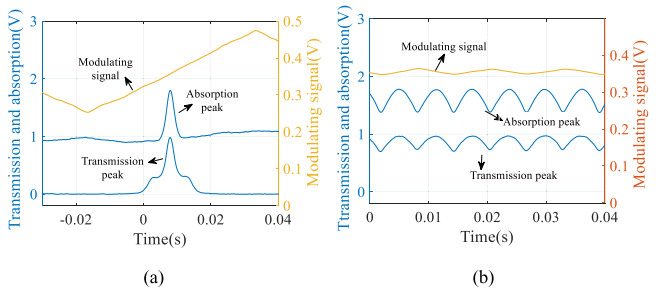


Fig. 4. Frequency stabilization results: (a) Complete absorption peak and transmission peak before frequency stabilization; (b) Absorption peak and transmission peak after frequency stabilization.

In the frequency stabilization unit, we employ the K atom's absorption peak at 43.0°C as the frequency reference. Upon initiating the operation of the frequency stabilization section, the FPGA first generates a full scales triangular wave signal through the DA circuit to modulate the frequency of the DFB laser. When the laser frequency resonates with the atoms, a noticeable change in laser power transmitted through the atomic vapor chamber results in the creation of an absorption peak. To enhance the clarity of the absorption peak, we employed two photodetectors, PD1 and PD2, for differential detection. The results from the differential amplifier are subsequently directed through an AD module and processed by the FPGA.

In Fig. 4(a), the entire K atomic absorption peak and the K-FADOF transmission peak are shown, both scanned by the modulation signal before frequency stabilization. The modulated signal is utilized to monitor the modulation voltage changes in the laser. The outcomes post-frequency stabilization is depicted in Fig. 4(b). We utilize a threshold to govern the extent of absorption peak scanning. A rising or falling edge of the modulation signal corresponds to the absorption peak, signifying the successful control of the laser's frequency within the specified threshold.

After conducting a comprehensive scan of the K atom absorption spectrum and the K-FADOF transmission spectrum, the FPGA is capable of detecting the absorption peak signal. It then records the position of the peak voltage and sets a threshold to preliminarily delineate a working frequency band centered around the peak. Subsequently, the FPGA, using the position of the peak voltage as the reference point, generates a triangular modulation signal with an amplitude of 10 V and a frequency of 11 Hz through the DA, continuously monitoring the voltage of the absorption peak. When the absorption peak voltage falls below the threshold, it indicates that the laser frequency has drifted away from the absorption peak. In response, the center frequency of the triangular modulation signal is adjusted until the absorption peak voltage returns to normal. The frequency stabilization module used in this study differs from traditional frequency stabilizers. Specifically, it implements a dynamic frequency locking function: the laser wavelength undergoes scanning, but the center of this scanning range is locked to the K atomic resonance absorption line. This dynamic frequency locking is necessary in optical systems utilizing FADOF because

FADOF exhibits high wavelength sensitivity. Without any frequency locking, even a slight laser wavelength drift of a few pm can cause a decrease in transmitted signal power, affecting the signal-to-noise ratio. By using this method, the background noise from light is eliminated and only the laser signal can pass through.

### C. Noise Generation

In an FMCW LiDAR system, the returning signal can be influenced by noise from both internal and external sources. Internal noise typically arises from phase fluctuations, such as natural noise of FMCW method from the local oscillator and optical circulator. External noise refers to interference caused by other energy sources outside the system. This kind of noise interference enters the signal processing system at the receiving end and disrupts the accurate extraction of frequency from the normal beat frequency signal.

External optical noise in a LiDAR system generally includes background light noise within the receiver's field of view. This encompasses sunlight scattering, sunlight reflection, direct sunlight, or other artificial light sources. Background light noise is characterized by a wide spectral range, random intensity fluctuations, and similarities with Gaussian noise in many aspects. Therefore, Gaussian noise is often used to simulate the intensity fluctuations of background light noise in various scenarios.

In order to investigate the impact of background light noise on LiDAR operation, we utilize an S2500E LED cold light source to generate optical noise. Its output is combined with the beat frequency signal of ranging and directed straight into the detector. To simulate the unpredictable fluctuations in background light noise, we use a voltage-controlled opto-electronic attenuator, whose attenuation rate is controlled by randomly varying voltage signal generated by an FPGA, to randomly decrease the intensity of the LED light. The temporal and spectral wave-forms of the background light noise generated using this method are depicted in Fig. 5(a) and (b), respectively. The probability distribution function (PDF) of the noise, as shown in Fig. 5(c), exhibits intensity values following a Gaussian distribution.

### D. Analyses of Indoor Results

In the indoor FMCW LiDAR ranging experiment, we conduct a validation test to assess the effectiveness of utilizing FADOF in suppressing background noise for a target positioned at a distance of 0.45 meters. PD3 is a silicon-based photodetector with a detection wavelength range spanning from 400 nm to 1100 nm. By removing the FADOF, we utilize an optical power meter to independently measure the averages of both noise power and beat frequency signal power before PD3. The noise power average is approximately 50.5 $\mu$W, while the beat frequency signal power hover around 67.8 $\mu$W. The experimental outcomes are recorded using a KEYSIGHT oscilloscope, capturing both the time-domain and frequency-domain signals at the receiving end.

Fig. 6(a) depicts the temporal waveform of the beat frequency signal when no back-ground light noise is present. From the spectrum plot in Fig. 6(b), it can be observed that the signal's

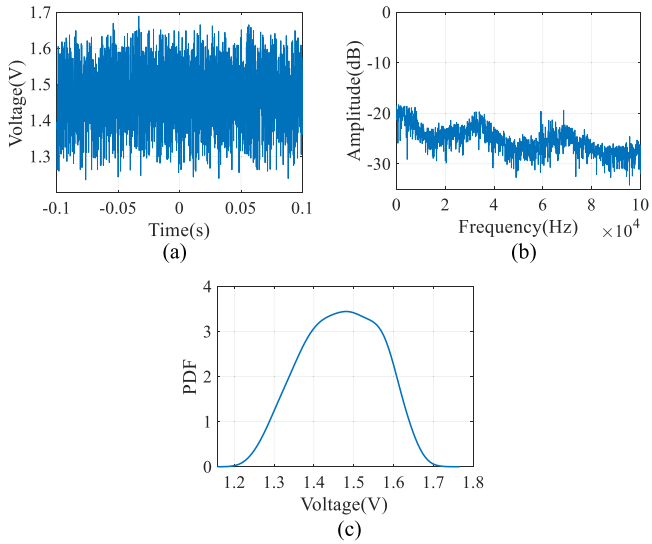


Fig. 5. Noise used in the indoor experiment: (a) Time domain signal of noise; (b) Frequency domain signal of noise. (c) Probability density function (PDF) of approximately Gaussian distribution noise.

frequency peak is at 272 Hz, corresponding to an amplitude of −10.3 dB in the frequency domain. In Fig. 6(c), the impact of added background light noise on the beat frequency signal is evident. Fig. 6(d) illustrates the frequency spectrum of the optical power signal detected by PD3 under the influence of noise interference. At this snapshot, noise results in an erroneous frequency peak at 343.8 Hz. Notably, this spectrum is continuously changing, making it impossible to accurately identify the correct frequency peak containing target distance information. This implies that while FMCW LiDAR's coherent reception mode possesses some noise resistance, strong background light can still disrupt its proper operation, underscoring the necessity to filter out background light noise.

Fig. 6(e) displays the temporal outcome of the beat frequency signal after filtering using K-FADOF. The waveform changes indicate the successful elimination of the erratic influence of background light noise on the echo signal's time domain. This effect is even more pronounced in Fig. 6(f), where the receiving system with K-FADOF successfully extracts the accurate frequency value of 272 Hz. In contrast to the −10.3 dB amplitude in Fig. 7(b), the signal amplitude is limited by FADOF's fixed transmittance, leading to a decrease to −14.7 dB. Measurement of the background light noise power passing through FADOF reveals its suppression to a level of 0.002 $\mu$W. These results are sufficient to demonstrate that FADOF can further bolster the FMCW LiDAR system's ability to withstand back-ground light noise, allowing it to operate effectively in even more challenging lighting conditions.

We can calculate the distance resolution and depth resolution. Distance resolution is the minimum distance that a system can resolve between two objects, commonly represented by the 3 dB bandwidth. In ideal conditions, it can be expressed by the following formula:

$$\Delta f = 2 * \frac{\Delta d}{c} * B * f_c. \tag{1}$$

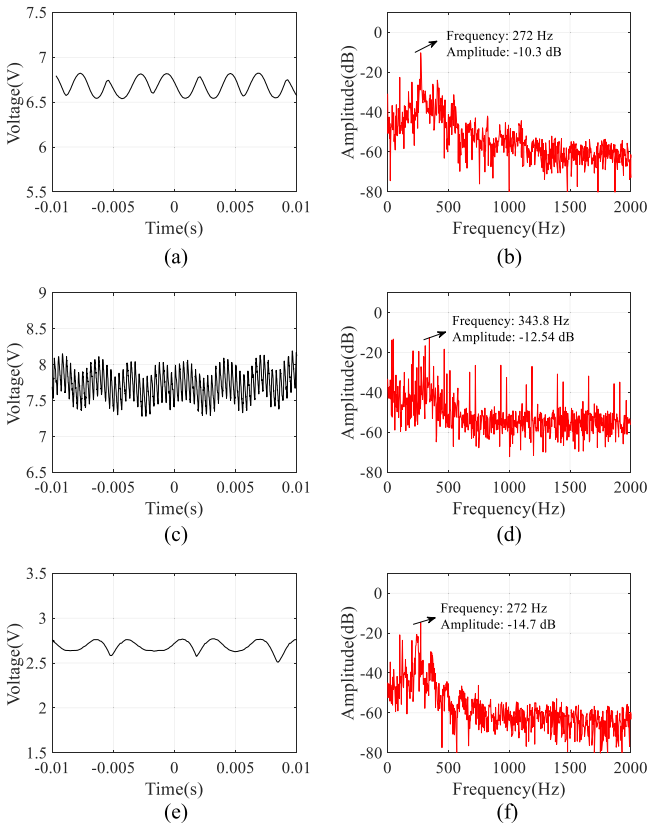


Fig. 6. Beat frequency signal without noise: (a) Time domain of the signal; (b) Frequency domain of the signal. Beat signal with noise added: (c) Time domain of the signal; (d) Frequency domain of the signal. Beat signal with FADOF at the receiver after noise added: (e) Time domain of the signal; (f) Frequency domain of the signal.

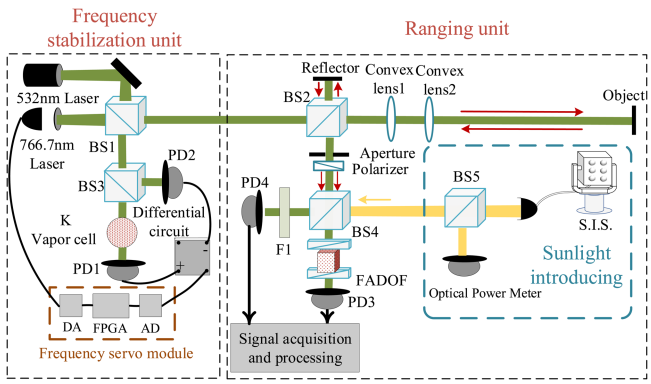


Fig. 7. Outdoor experimental setup. BS1, BS2, BS3, BS4, and BS5 represent beam splitters. PD1, PD2, PD3, and PD4 represent photodetectors. S.I.S. represents a Sunlight introducing system. F1 represents a 10 nm filter.

In (1), we have $\Delta f$ representing frequency, $\Delta d$ representing distance, $B$ representing the laser's frequency modulation bandwidth, and $f_c$ representing the modulation frequency. With the modulation frequency being constrained by $\Delta f$, the simplification of distance resolution follows:

$$\Delta D = \frac{c}{2B}. \tag{2}$$

Depth resolution is connected to frequency resolution through its relationship with sampling time.

$$\Delta f_{\min} = \frac{1}{T} = \frac{F_s}{N}. \tag{3}$$

$\Delta f_{min}$ stands for frequency resolution, where $T$ denotes the sampling time, $F_s$ stands for the sampling frequency, and $N$ represents the number of sampling points. By combining (1) and (3), we can derive the depth resolution.

$$\Delta d_{\min} = \frac{c}{2B * f_c} * \frac{F_s}{N}. \tag{4}$$

Before frequency locking, the frequency modulation bandwidth of the laser is 15 GHz and the modulation frequency is 11 Hz. At this time, the voltage of the highest transmission spectrum is 0.98V. We can achieve a distance resolution of 1 cm and a depth resolution of 0.14 cm. Similarly, we can infer the performance of LiDAR under dynamic frequency locking conditions. Following frequency stabilization, the laser's tuning bandwidth is 0.56 GHz, corresponding to a modulation frequency of 80 Hz. Consequently, the frequency stabilization leads to a reduction in distance resolution to 27 cm, equating to a depth resolution of 0.5 cm. Generally speaking, distance resolution and depth resolution jointly determine the resolution of LiDAR. From this analysis, it is evident that the laser's tuning bandwidth is considerably narrower than the laser diode's full mode-hop-free tuning range of 50 GHz, leading us to conclude that the behavior is approximately linear within this limited span. Given that this study primarily focuses on the beneficial impact of FADOF on the resistance of FMCW LiDAR systems to light noise, and considering that the frequency modulation linearity of the 766.7 nm laser does not significantly relate to the main conclusions, we did not delve further into the discussion on the laser linearity.

## III. Outdoor Experiment

Through indoor LiDAR experiments, we have drawn two preliminary conclusions. First, strong background noise from ambient light can adversely affect the normal operation of FMCW LiDAR systems. Second, FADOF proves effective in enhancing the system's resistance to background light noise. Following this, we set up an outdoor environment to conduct experiments on an FMCW LiDAR system under direct sunlight, testing the performance of FADOF under realistic strong background light interference conditions.

The outdoor experimental setup closely resembles the indoor setup, with three key modifications, as illustrated in Fig. 7. Firstly, the 766.7 nm laser is challenging to perceive in outdoor conditions, so we introduce a 532 nm guiding light path to overlap the two laser signals, facilitating optical setup. Secondly, the noise generation module used indoors is replaced with a real Sunlight introducing module. Thirdly, we add a reference light path after BS4, incorporating a 10 nm filter to eliminate

background light noise. This is done to compare the filtering effectiveness of FADOF.

### A. Sunlight Introduction System

In contrast to indoor experiments employing FPGA simulations to analyze noise fluctuations, outdoor experiments involve the collection of ambient noise through a Sunlight Introducing System (S.I.S.). The S.I.S., illustrated in Fig. 7, comprises six large lenses connected to six fibers, consolidating the gathered sunlight into a single fiber for output. Through voltage adjustments, the sunlight collection system can autonomously calibrate its angle to align with the sun and make minute adaptations as the sun's position changes. This ensures optimal sunlight collection at all times. In practical scenarios, given the potential intensity of sunlight, all six fibers are not always utilized for collection. Depending on the initial sunlight strength when fibers are connected, we employ 2 to 6 fibers during the formal collection phase to prevent potential damage to the devices.

Once sunlight is gathered by the sunlight collection system, we split it using BS5, measuring a segment with a power meter to quantify sunlight noise. The remaining sunlight is then evenly distributed into two paths, the one with FADOF and the other one with 10 nm filter, through BS4. To ensure uniform light noise reception on both paths, we implement measures to minimize the influx of extraneous daylight noise during the noise introduction process. This includes covering experimental equipment and guaranteeing that all noise originates solely from the sunlight introducing module.

### B. Data Collection

The outdoor experiment is conducted in front of a teaching building, and due to the building obstruction, the period when it can be illuminated by the sun is roughly from 10 A.M. to 5 P.M. The sunlight introduction system, capable of tracking the sun's movement, ensures that during this time frame, the experimental system consistently operates under conditions equivalent to direct sunlight.

For outdoor experiments, we use a slower but programmable AD sampling module to enable long-term automated data storage, with a sampling rate of 20k Hz. Ranging measurements are taken every 10 minutes, each lasting 10 seconds. In this case, the data collected in one day amounts to hundreds of mega-bytes, which puts minimal strain on electronic devices. We then divide the sampled signal into 10 parts, with each part having a sampling time of 1 s, to obtain 10 beat frequency peaks with a spectral accuracy of at least 1 Hz, which improves with FFT zero padding. Afterwards, we calculate the average of these 10 values as the result of each ranging measurement.

Both the FADOF filter path and the 10 nm filter path are simultaneously collected, utilizing the aforementioned data processing method. As sunlight background noise fluctuates throughout the day, the results of the two ranging paths are influenced differently by the noise. This allows us to evaluate and validate the differences between FADOF and traditional filtering approaches.

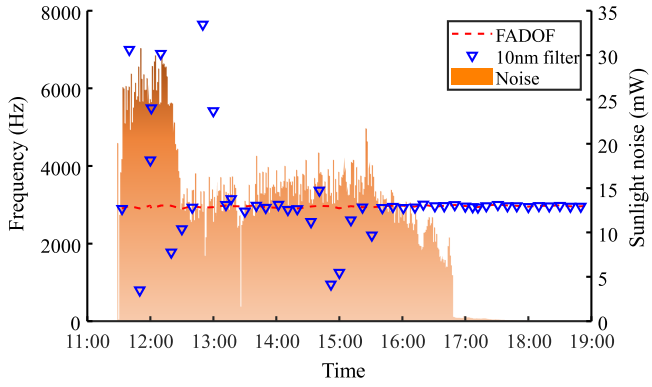


Fig. 8. Continuous collection of sunlight noise throughout the day, and the ranging results obtained through FADOF filtering and 10 nm filter filtering.

### C. Outdoor Results and Discussion

We conduct an outdoor ranging experiment on September 3, 2023. In this experiment, the target object is a corner cube prism coated with aluminum film, with a diameter of 64 mm. Its reflectivity for most wavelengths of laser light reaches above 70%. However, there is an absorption peak near 800 nm, making the actual reflectivity for a 766.7 nm laser around 55%. The target distance is approximately 5 meters, corresponding to a beat frequency peak of around 2980 Hz. After preparing for the experiment, we officially start around 11:30 in the morning and conclude around 7:00 in the evening. During the experiment, the average power of the signal entering the receiver is 0.11 mW, while the optical noise power consistently fluctuates.

The test results are shown in Fig. 8. The figure includes the monitored sunlight power incident on the system, the beat frequency signal spectrum peak values for the FADOF filter path, and the 10 nm filter path. Due to the different optical paths between the power meter and the PD receiver, the noise received by the power meter and the noise actually received before the filters inevitably have some differences. However, since the beam splitters and the experimental optical path are fixed, the proportion between them can be considered constant. The sunlight power monitoring results can be used to indicate the intensity of sunlight noise reaching the receiver. From the Fig. 8, it can be observed that the power of sunlight noise fluctuates throughout the day, so ranging results at different noise levels can be obtained.

We perform FFT transformation on the obtained beat frequency signals to obtain frequency spectra and conduct Voigt function fitting to extract peak frequencies from the fitted curve. For the beat frequency results using the 10 nm filter, effective peak values cannot be obtained once the noise reaches a certain level. When monitoring sunlight power above 15 mW, the peak of the fitted curve is highly unstable, making it impossible to obtain accurate distance information. It is only when monitoring sunlight power below 15 mW that fitting can yield relatively valid peak results, and accuracy increases when below 13 mW. For the FADOF filter path, due to its powerful out-of-band suppression, it effectively reduces the impact of sunlight noise,

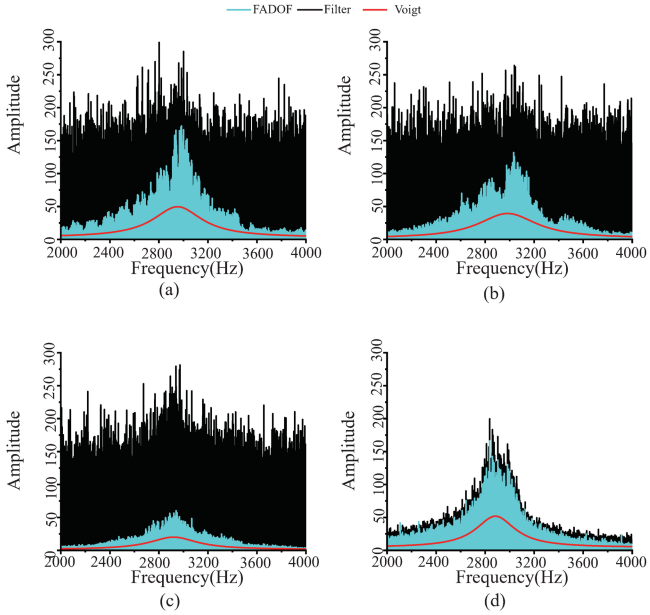


Fig. 9. Spectral graphs of LiDAR results when filtered through a 10 nm filter or FADOF under varying noise levels: (a) 16 mW noise; (b) 14 mW noise; (c) 12.3 mW noise; (d) 0.004 mW noise.

yielding stable peak results and accurate distance measurements throughout the entire experiment.

Fig. 9 illustrates a portion of the collection results from September 3rd. The black section in the figure represents the outcome after traditional filter application, the cyan portion signifies the outcome after employing FADOF, and the red line depicts peak extraction using the Voigt function. Fig. 9(a)–(d) respectively showcase the outcomes of FADOF and 10 nm filter when the noise levels are at 16 mW, 14 mW, 12.3 mW, and 0.004 mW.

It becomes apparent that in Fig. 9(d), the signals of both 10 nm filter and FADOF are essentially similar due to the noise being close to 0. In Fig. 9(c), with the noise reaching 12 mW, it overwhelms most of the signal, and optimal peak results can only be obtained when the fitting range is narrow. In Fig. 9(b), as the noise gradually increases from 12 mW to 16 mW, the filtered signal spectrum, under the influence of noise, becomes higher and higher at the bottom, eventually burying the signal. Meanwhile, FADOF remains largely unaffected. In instances of extreme noise influence, the noise can even reach the saturation absorption point of the photodetector, causing the received signal to distort completely.

After finishing a full day of ranging experiments on September 21, 2023, we decide to test the farthest distance the current LiDAR system can measure. To keep things consistent, we still use the corner-reflecting prism with the same settings as the experiment on September 3rd. However, to reach greater distances, we tweak the stabilized laser parameters, setting the bandwidth to 0.6 GHz and the frequency modulation period to 10 Hz. This gives us a distance resolution of 25 cm and a depth resolution of 1.25 cm. We push the distance further, placing the target about 17 meters away. Fig. 10 shows the results for the FADOF filter path. The average power of the signal entering the

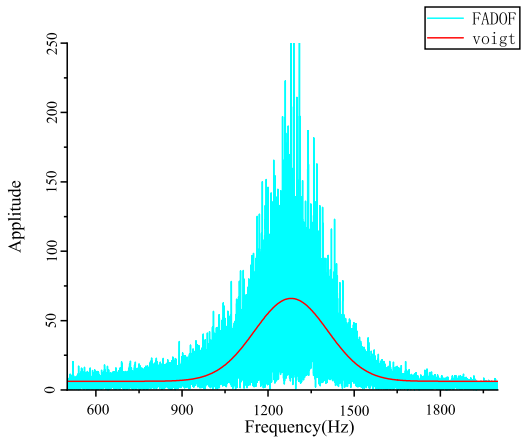


Fig. 10. Spectrum results of the LiDAR with FADOF, when the target is located 17 meters away.

receiver is roughly 0.15 mW, with the laser reflected by the target object at about 0.02 mW and the local reference laser at 0.13 mW. The input noise power is approximately 83 mW. The outcome is similar to the full-day ranging experiment. Even when exposed to strong sunlight noise, the beat frequency signal after FADOF filtering remains largely unaffected. It still accurately picks out the correct peak frequency through Voigt curve fitting, allowing for distance measurement. This suggests that our experimental system can measure distances of at least 17 meters under direct sunlight conditions.

It's worth mentioning that our limitations aren't due to noise but rather the lack of certain experimental instruments and equipment. The 766.7 nm laser we're using was originally meant for atomic physics experiments and isn't optimized for long-distance sensing. Moreover, we lack specific transmitting and receiving optical antennas; instead, our optical system is built with just two simple convex lenses. In other words, the experimental setup described in this paper is only designed as a basic system to validate the functionality of FADOF in resisting strong background light. It's quite different from practical LiDAR systems. Therefore, many LiDAR-related parameters, such as detection distance, FoV, frequency modulation linearity, etc., still have significant room for improvement.

## IV. Conclusion

The performance of the FMCW LiDAR system is significantly influenced by the tuning bandwidth. Generally, a wider tuning bandwidth tends to improve distance resolution [28], [29]. The inherent narrow bandwidth characteristic of FADOF enhances the system's ability to counter optical noise. However, this narrower tuning bandwidth also results in reduced ranging resolution. Striking a balance between these performance aspects becomes crucial, depending on the actual operating environment of the system.

In extremely strong background light noise environments, obtaining any effective beat frequency values without using FADOF for filtering becomes challenging. Introducing FADOF in such situations allows the FMCW laser ranging system to

sacrifice a certain level of resolution but still function adequately in extreme environments with strong background noise.

In this study, in order to verify the impact of FADOF on the background noise resistance performance of the FMCW LiDAR system, we set up a simple FMCW LiDAR system in the 766.7 nm wavelength range that matches the K atom D2 line wavelength. By applying K-FADOF for optical noise filtering at the receiver end of the system, the FMCW LiDAR system is able to regain its capability to measure target distances. In indoor experiments, after introducing strong and randomly varying broadband background noise, the FMCW LiDAR system without optical noise filtering is unable to function properly. In outdoor experiments, the differences in filtering capabilities become more apparent. As the noise from sunlight gradually increases, the signal will gradually be covered by the noise signal, eventually disappearing completely.

The experimental results confirm the feasibility of using FADOF to enhance the background noise resistance of the FMCW LiDAR system. In the 766.7 nm wavelength band achieved in this study, numerous LiDAR applications exist, such as temperature measurement LiDAR in the field of earth's middle atmosphere research [22]. The outcomes of this study may enhance the performance of corresponding LiDAR systems in these fields. Furthermore, similar conclusions can be extended to other wavelength ranges where FADOF can be produced and there exists a matching laser source. For instance, Rb-ESFADOF operating at 1529 nm wavelength with corresponding 1550 nm laser sources represents a more mature and practical wavelength band in FMCW LiDAR research. In strong noise environment, this system can work effectively, so this work holds the potential to expand the application scenarios of FMCW LiDAR.

## References


[1] P. F. McManamon, "Review of ladar: A historic, yet emerging, sensor technology with rich phenomenology," *Opt. Eng.*, vol. 51, no. 6, 2012, Art. no. 060901.

[2] A. Swatantran, H. Tang, T. Barrett, P. DeCola, and R. Dubayah, "Rapid, high-resolution forest structure and terrain mapping over large areas using single photon lidar," *Sci. Rep.*, vol. 6, no. 1, 2016, Art. no. 28277.

[3] K. Lim, P. Treitz, M. Wulder, B. St-Onge, and M. Flood, "LiDAR remote sensing of forest structure," *Prog. Phys. Geogr.-Earth Environ.*, vol. 27, no. 1, pp. 88–106, 2003.

[4] M. Jaboyedoff et al., "Use of LIDAR in landslide investigations: A review," *Natural Hazards*, vol. 61, no. 1, pp. 5–28, 2012.

[5] G. Baumgarten, "Doppler Rayleigh/Mie/Raman lidar for wind and temperature measurements in the middle atmosphere up to 80 km," *Atmosph. Meas. Techn.*, vol. 3, no. 6, pp. 1509–1518, 2010.

[6] B. Schwarz, "Mapping the world in 3D," *Nature Photon.*, vol. 4, no. 7, pp. 429–430, 2010.

[7] A. Martin et al., "Photonic integrated circuit-based FMCW coherent LiDAR," *J. Lightw. Technol.*, vol. 36, no. 19, pp. 4640–4645, Oct. 2018.

[8] E. W. Mitchell et al., "Coherent laser ranging for precision imaging through flames," *Optica*, vol. 5, no. 8, pp. 988–995, 2018.

[9] Y. Wu, L. Deng, K. Yang, and W. Liang, "Narrow linewidth external cavity laser capable of high repetition frequency tuning for FMCW LiDAR," *IEEE Photon. Technol. Lett.*, vol. 34, no. 21, pp. 1123–1126, Nov. 2022.

[10] Z. Xu, H. Zhang, K. Chen, D. Zhu, and S. Pan, "FMCW lidar using phase-diversity coherent detection to avoid signal aliasing," *IEEE Photon. Technol. Lett.*, vol. 31, no. 22, pp. 1822–1825, Nov. 2019.

[11] D. J. Lum, S. H. Knarr, and J. C. Howell, "Frequency-modulated continuous-wave LiDAR compressive depth-mapping," *Opt. Exp.*, vol. 26, no. 12, pp. 15420–15435, 2018.

[12] S. Ayhan, S. Scherr, A. Bhutani, B. Fischbach, M. Pauli, and T. Zwick, "Impact of frequency ramp nonlinearity, phase noise, and SNR on FMCW radar accuracy," *IEEE Trans. Microw. Theory Techn.*, vol. 64, no. 10, pp. 3290–3301, Oct. 2016.

[13] H. Tian, W. Chang, X. Li, and Z. Liu, "Strong spurious noise suppression for an FMCW SAR," *Radio Eng.*, vol. 25, no. 3, pp. 581–591, 2016.

[14] K. Siddiq, M. K. Hobden, S. R. Pennock, and R. J. Watson, "Phase noise in FMCW radar systems," *IEEE Trans. Aerosp. Electron. Syst.*, vol. 55, no. 1, pp. 70–81, Feb. 2019.

[15] R. Wang, M. Xiang, and C. Li, "Denoising FMCW ladar signals via EEMD with singular spectrum constraint," *IEEE Geosci. Remote Sens. Lett.*, vol. 17, no. 6, pp. 983–987, Jun. 2020.

[16] B. Yin and T. M. Shay, "Faraday anomalous dispersion optical filter for the Cs 455 nm transition," *IEEE Photon. Technol. Lett.*, vol. 4, no. 5, pp. 488–490, May 1992.

[17] H. Guo, A. Dang, Y. Han, B. Luo, S. Gao, and Y. Cao, "Faraday anomalous dispersion optical filter," *Chin. Sci. Bull.*, vol. 55, no. 7, pp. 527–533, 2010.

[18] W. Kiefer, R. Löw, J. Wrachtrup, and I. Gerhardt, "Na-faraday rotation filtering: The optimal point," *Sci. Rep.*, vol. 4, no. 1, 2014, Art. no. 6552.

[19] S. D. Harrell et al., "Sodium and potassium vapor Faraday filters revisited: Theory and applications," *J. Opt. Soc. Amer. B*, vol. 26, no. 4, pp. 659–670, 2009.

[20] B. Luo, L. Yin, J. Xiong, J. Chen, and H. Guo, "Induced-dichroism-Excited atomic line filter at 1529 nm," *IEEE Photon. Technol. Lett.*, vol. 30, no. 17, pp. 1551–1554, Sep. 2018.

[21] H. Chen, M. A. White, D. A. Krueger, and C. Y. She, "Daytime mesopause temperature measurements with a sodium-vapor dispersive Faraday filter in a lidar receiver," *Opt. Lett.*, vol. 21, no. 15, pp. 1093–1095, 1996.

[22] J. Höffner and C. Fricke-Begemann, "Accurate lidar temperatures with narrowband filters," *Opt. Lett.*, vol. 30, no. 8, pp. 890–892, 2005.

[23] J. Tang et al., "Experimental study of a model digital space optical communication system with new quantum devices," *Appl. Opt.*, vol. 34, no. 15, pp. 2619–2622, 1995.

[24] T. Shi et al., "A dual-frequency Faraday laser," *IEEE Photon. J.*, vol. 12, no. 4, Aug. 2020, Art. no. 1503211.

[25] L. Yin, D. Qian, Z. Geng, H. Zhan, and G. Wu, "Using FADOF to eliminate the background light influence in ghost imaging," *Opt. Exp.*, vol. 30, no. 20, pp. 36297–36306, 2022.

[26] M. A. Zentile, J. Keaveney, L. Weller, D. J. Whiting, C. S. Adams, and I. G. Hughes, "ElecSus: A program to calculate the electric susceptibility of an atomic ensemble," *Comput. Phys. Commun.*, vol. 189, pp. 162–174, 2015.

[27] J. Keaveney, C. S. Adams, and I. G. Hughes, "ElecSus: Extension to arbitrary geometry magneto-optics," *Comput. Phys. Commun.*, vol. 224, pp. 311–324, 2018.

[28] J. Zheng, "Analysis of optical frequency-modulated continuous-wave interference," *Appl. Opt.*, vol. 43, no. 21, pp. 4189–4198, 2004.

[29] Z. Lu, C. Ge, Z. Wang, D. Jia, and T. Yang, "Basics and developments of frequency modulation continuous wave LiDAR," *Opto-Electron. Eng.*, vol. 46, no. 7, 2019, Art. no. 190038.